



Nanoscale

**Polysalt Ligands Achieve Higher Quantum Yield and Improved Colloidal Stability for CsPbBr<sub>3</sub> Quantum Dots**

Journal:	<i>Nanoscale</i>
Manuscript ID	NR-ART-07-2021-004753.R1
Article Type:	Paper
Date Submitted by the Author:	05-Sep-2021
Complete List of Authors:	Wang, Sisi; Florida State University, Department of Chemistry and Biochemistry and Integrative Nanoscience Institute Du, Liang; Florida State University, Department of Chemistry and Biochemistry Donmez, Selin; Florida State University, Department of Chemistry and Biochemistry Xin, Yan; Florida State University, NHMFL Mattoussi, Hedi; Florida State University, Department of Chemistry and Biochemistry

SCHOLARONE™  
Manuscripts

## Polysalt Ligands Achieve Higher Quantum Yield and Improved Colloidal Stability for CsPbBr<sub>3</sub> Quantum Dots

Sisi Wang,<sup>1</sup> Liang Du,<sup>1</sup> Selin Donmez,<sup>1</sup> Yan Xin<sup>®</sup> and Hedi Mattoussi<sup>1,\*</sup>

<sup>1</sup> Florida State University, Department of Chemistry and Biochemistry, 95 Chieftan Way, Tallahassee, FL 32306

<sup>®</sup> Florida State University, National High Magnetic Field Laboratory, 1800 E. Paul Dirac Drive, Tallahassee, Florida, 32310

\* Email: mattoussi@chem.fsu.edu

### Abstract:

Colloidal lead halide perovskite quantum dots (PQDs) are relatively new semiconductor nanocrystals with great potential for use in optoelectronic applications. They also present a set of new scientifically challenging fundamental problems to investigate and understand. One of them is to address the rather poor colloidal and structural stability of these materials under solution phase processing and/or transfer between solvents. In this contribution, we detail the synthesis of a new family of multi-coordinating, bromide-based polysalt ligands and test their ability to stabilize CsPbBr<sub>3</sub> nanocrystals in polar solutions. The ligands present multiple salt groups involving quaternary cations, namely ammonium and imidazolium as anchors for coordination onto PQD surfaces, along with several alkyl chains with varying chain length to promote solubilization in various conditions. The ligands provide a few key benefits including the ability to repair damaged surface sites, allow rapid ligand exchange and phase transfer, and preserve the crystalline structure and morphology of the nanocrystals. The polysalt-coated PQDs exhibit near unity PLQY and significantly enhanced colloidal stability in ethanol and methanol.

**Keywords:** Perovskite nanocrystals, surface stabilization, polymer ligands, quaternary ammonium, imidazolium anchors, PL quantum yield, colloidal stability

## INTRODUCTION

Colloidal all-inorganic lead halide  $\text{CsPbX}_3$  ( $X = \text{Cl}, \text{Br}, \text{I}$ ) perovskite quantum dots, PQDs, have generated enormous interest in recent years.<sup>1-4</sup> Those interests are motivated by some of their unique photophysical properties, such as tunable bandgap, high photoluminescence quantum yield (PLQY) and narrow emission profiles, all combined with easy to implement solution phase synthesis and processing.<sup>5-6</sup> These materials are very promising for use in optoelectronic applications, including solar cell technology,<sup>7-10</sup> light-emitting diodes (LED),<sup>11-13</sup> liquid crystal display (LCD),<sup>14</sup> photodetectors<sup>15</sup> and scintillators.<sup>16</sup> In addition, PQDs exhibit high tolerance to structural defects, as rather shallow energy traps characterize these materials, a property traced to the orbital composition of the energy bands calculated for lead halide perovskites.<sup>2, 17</sup> However, a major hurdle that has inhibited implementation of those promising applications and slowed the in-depth characterization of these materials (structure, optical and electronic properties) has been their rather limited colloidal and structural stability, compared to the more “conventional” colloidal quantum dots made of metal chalcogenide cores. Some of these problems emanate from the ionic nature of the core crystals, which yield low internal lattice energy, a highly dynamic ligand binding onto the nanocrystal surfaces and limited structural stability in polar solutions.<sup>18-19</sup>

In a typical growth reaction of colloidal perovskite nanocrystals, a combination of alkyl acid (oleic acid, OA) and alkyl base (oleylamine, OLA) are used to form the metal-organic precursors and eventually surface stabilize the as-grown NCs in non-polar media.<sup>5</sup> Those ligands interact with the nanocrystals in the form of primary ammonium ( $\text{OLA}^+$ , hard Lewis acid) and carboxylate ( $\text{OA}^-$ , hard Lewis base) ion pairs, and they exhibit rather weak affinity to the NC surfaces, which result in high rate of ligand desorption and reduced colloidal stability.<sup>19</sup> Additionally, it has been suggested that proton transfer between oleate and oleylammonium ions (in solution) can neutralize the surface-bound oleylammonium species, further weakening ligand affinity to the PQD surfaces.<sup>18-20</sup> These factors make solution phase grown PQDs very sensitive to solvent polarity. For example, a few rounds of precipitation using a non-solvent can induce loss of structural integrity, colloidal instability, coupled with a drop of fluorescence.<sup>21-22</sup> This indicates that solution processing would increase the density of structural defects (mostly surface-located), often associated with large surface-to-volume ratio of the nanocrystals and rather poor electronic passivation provided by weakly binding native ligands.<sup>21, 23</sup> Consequently, the nature of the surface coating chemistry applied to stabilize these materials plays an important role in every aspect of

their behavior, including colloidal stability, photophysical characteristics, carrier transport properties and the ability to carry out solution processing of the nanocrystals into thin film devices.<sup>24-25</sup>

Several studies have attempted to address the above limitations by identifying novel coatings that exhibit higher binding affinity to the PQD surfaces and better electronic passivation of defect states. Kovalenko and co-workers introduced zwitterionic-containing molecules such as alkyl sulfobetaine or phosphocholine derivatives during the growth reaction, to alter the composition of the final nanocrystal coating.<sup>26-27</sup> They reported that this strategy yielded QDs with better colloidal and structural stability under high dilution conditions and anti-solvent washes. Other groups including Manna and co-workers, Sun and co-workers, and Zeng and co-workers have substituted OLA/OA with alkyl phosphonic acid or benzenesulfonic acid as surfactants during synthesis, and reported the growth of PQDs with enhanced PLQY and better stability under few rounds of purification or under diluted conditions.<sup>28-31</sup> This improvement was attributed to the higher affinity of phosphonate groups to  $\text{Pb}^{2+}$  surface ions. As an alternative strategy to introducing new surfactants during growth, Alivisatos' group and Samanta's group implemented post growth treatment of the PQDs as a means of improving PLQY and colloidal stability. Post-treatment of PQDs with inorganic salts, such as thiocyanate and tetrafluoroborate, or alkyl phosphonate, were used to passivate under-coordinated surface  $\text{Pb}^{2+}$  sites, resulting in better fluorescence properties.<sup>32-34</sup> Another actively explored idea involves the use of didodecyl ammonium bromide (DDAB) as surface passivating ligands, which were either introduced during preparation or applied post-growth to the PQDs.<sup>13, 22, 35-46</sup> Despite these successes, rather modest progress has been realized using these various small molecule ligands, due to both lingering weak binding and modest steric stabilization of the PQDs.

In this report, we probe the capacity of a set of multidentate polysalt polymers based on the quaternary ammonium or imidazolium motifs to provide stable coating and simultaneously improve the PL emission of colloidal perovskite quantum dots. The ligand design exploits the highly efficient nucleophilic addition reaction between amine-bearing blocks (as nucleophiles) and succinic anhydride rings in a low molecular weight poly(isobutylene-alt-maleic anhydride), PIMA, copolymer.<sup>47-50</sup> The resulting compounds present several copies of either alkyl ammonium or imidazolium (as bromide salt groups) for electrostatic coordination onto the PQDs, along with multiple alkyl chains with varying length ( $\text{C}_8$  or  $\text{C}_{18}$ ) to ensure expanded affinity of the polysalt-

ligated nanocrystals to organic solvents with varying properties. Ligand substitution of OLA/OA-capped CsPbBr<sub>3</sub> PQDs with these polysalts yielded NCs with significant enhancement in the PLQY, preserved absorption profiles and much better colloidal stability in polar media. X-ray powder diffraction (PXRD) combined with transmission electron microscopy (TEM) data confirmed that the integrity of the crystal structure and nanocrystal shape were essentially unaffected by the ligand substitution. Furthermore, we utilized nuclear magnetic resonance (NMR) to track changes in the surface coatings, proving that a complete ligand exchange is achieved. Dynamic light scattering (DLS) measurements showed that homogenous dispersions that are free of aggregates characterize the PQD colloids. Last, the stability of the nanocrystals was evaluated using anti-solvent solution processing, probing resistance of the PQDs to water and easy phase transfer to polar solvents, including ethanol and methanol, without altering the nanocrystal integrity or optical properties of the materials even after extended storage.

## RESULTS AND DISCUSSION

### Rationale

There is a consensus in the community that the documented rapid degradation of the as-grown lead-halide-based PQDs is initiated by etching of the nanocrystal surfaces during incubation and processing. This etching is facilitated by the ionic nature of the QD cores, and it tends to alter the surface structure as well as the integrity of the nanocrystals. We thus reasoned that designing a high affinity protective coating that presents several halide salt groups per ligand would competitively displace the native labile cap of the nanocrystals and progressively repair damaged sites, by sharing the halide ions with the QD surfaces. This would also improve the fluorescence quantum yields of the compounds.<sup>33</sup> Synthesis of the polysalts exploits the efficiency of the nucleophilic addition reaction between distinct amine-R nucleophiles and poly(isobutylene-alt-maleic anhydride) block copolymer, to design several high affinity coordinating ligands that are ideally adapted for stabilizing luminescent chalcogenide quantum dots and other transition metal nanoparticles.<sup>47-49, 51-52</sup> Here, we use quaternary ammonium bromide or imidazolium bromide salts as coordinating groups onto PQD surfaces and alkyl chains to promote solubility in various organic and polar media. **Figure 1A** summarizes the general synthetic strategy for preparing our polysalts, where two steps are involved. Two distinct nucleophile precursors are combined for each set of ligands, namely N,N-dimethylaminopropylamine (AM) or 1-(3-Aminopropyl)imidazole (IM) is

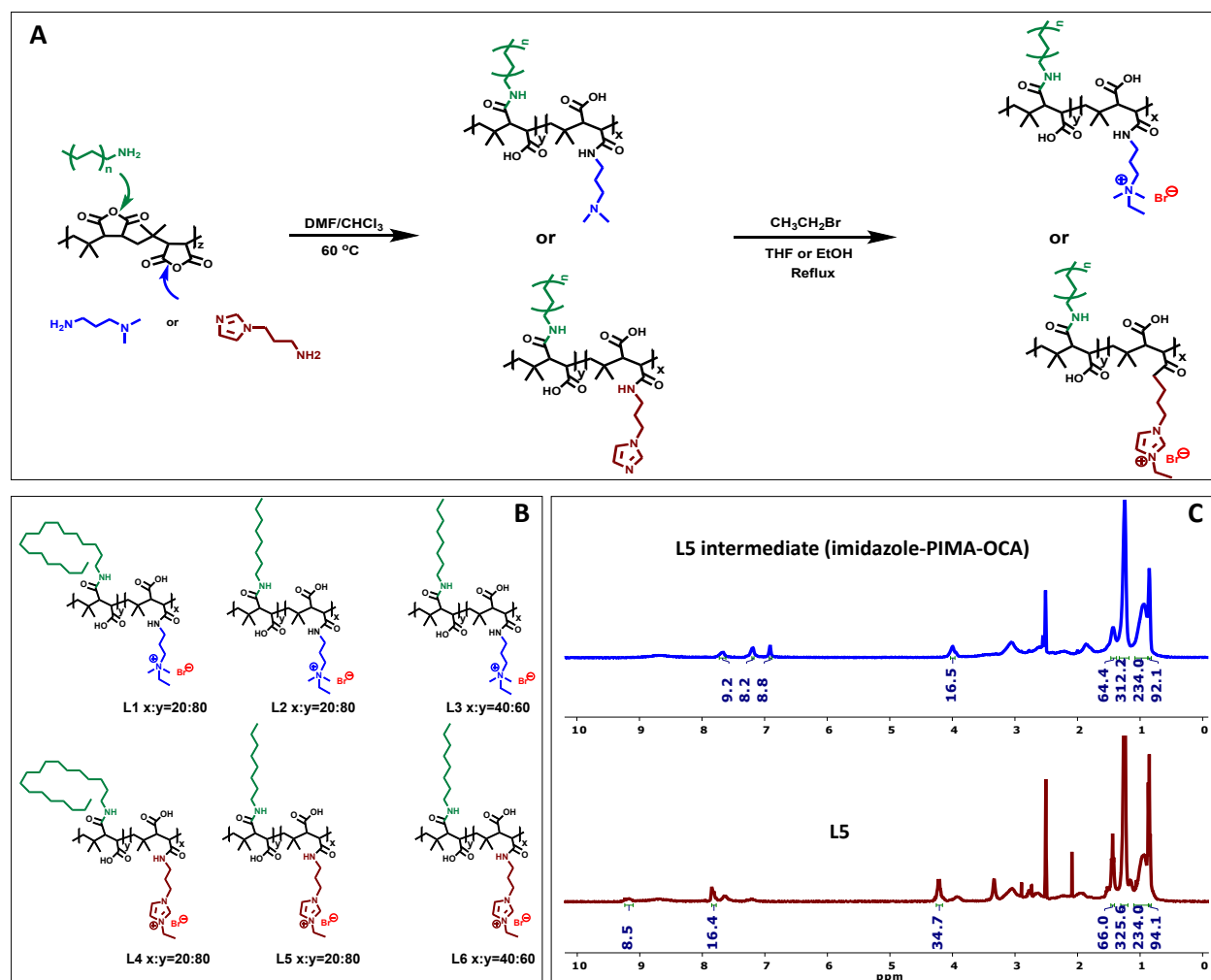


**Figure 1:** (A) Schematic representation of the nucleophilic addition reaction used to prepare the polysalt ligands. (B) Structures and nomenclature of the ligands prepared and tested in this study. (C) <sup>1</sup>H NMR spectra collected from imidazole-PIMA-OCA (intermediate, top) and the corresponding imidazolium-PIMA-OCA polysalt L5 (bottom). Both compounds were dissolved in DMSO-d<sub>6</sub>.

used as salt source, while octylamine (OCA) or octadecylamine (ODA) provides the solubilizing alkyl chains. In a typical reaction, AM or IM is mixed with a PIMA solution in DMF. Then, OCA in DMF or ODA pre-dissolved in CHCl<sub>3</sub> is added to the mixture, which was heated to ~60 °C, and left to react overnight while stirring. Then, the tertiary amine or imidazole groups are transformed into quaternary ammonium (AMB) or imidazolium (IMB) salts by reaction with bromoethane. The final products display several salt groups installed randomly along the polymer backbone (as schematically depicted in **Figure 1**). Taking advantage of the versatility of this strategy, we synthesized six sets of polysalts with well-defined stoichiometry. Three ligands present AMB

groups: **L1** (AMB:ODA = 20:80); **L2**: (AMB:OCA = 20:80); **L3**: (AMB:OCA = 40:60); and three present IMB groups: **L4** (IMB:ODA = 20:80); **L5** (IMB:OCA = 20:80); **L6** (IMB:OCA = 40:60), see **Table 1** and **Figure 1**. Here, x and y designate the molar fraction of anchoring groups and solubilizing chains estimated with respect to the monomer concentration of the PIMA (there are ~40 monomers per chain). As an example, synthesis of **L1** was carried out by reacting PIMA with a mixture of N, N-dimethylaminopropylamine and octadecylamine at 20:80 molar ratio, then followed by quaternization reaction alkylating the tertiary amine into alkyl ammonium bromide (AMB). Conversely, synthesis of ligand **L6** was carried out by reacting PIMA with 1-(3-aminopropyl)imidazole and octylamine at a molar ratio 40:60, and then transforming the imidazole into imidazolium bromide (IMB) in the presence of bromoethane. Further details about the synthetic steps are provided in the **ESI**. The  $^1\text{H}$  NMR data shown in **Figure 1** and **ESI (Figures S1-S3)** confirm the successful preparation of the various ligands with the desired structures. For instance, the spectra acquired for IMB-PIMA-OCA show peaks at ~9.2 ppm and ~7.9 ppm characteristic of the imidazolium protons, while the peaks at ~0.85 ppm and ~1.24 ppm are respectively ascribed to the terminal  $-\text{CH}_3$  and  $-\text{CH}_2$  groups of octylamine. In addition, a broad peak centered at ~0.95 ppm ascribed to the methyl protons along the polymer backbone was also measured. The degree of grafting was estimated by comparing the integration values of the  $^1\text{H}$  NMR peaks of different moieties; details are listed in **Table 1**. It should be noted that the salt-to-ODA molar ratio could not be determined with good accuracy, due to broadening of the peaks and a pronounced overlap between the signatures of the ODA and PIMA methyl protons in the NMR spectrum. Nevertheless, quantification of the number of anchors and OCA chains in the other polysalts is indicative of good agreement between the nominal and measured stoichiometry values for the synthesized compounds (see **Table 1**). This agrees with prior studies, which have shown that the addition reaction yields polymers with stoichiometry that is very close to that anticipated from the nominal values based on the molar concentrations of the nucleophile precursors.<sup>49, 52</sup>

### Ligand Exchange and Phase Transfer

$\text{CsPbBr}_3$  nanocrystals, grown via the hot injection method using oleic acid and oleylamine ligands (OLA/OA-PQDs), were used for testing the ability of the polysalt ligands to achieve high binding affinity, repair defect sites and provide electronic passivation.<sup>5</sup> Considering the different solubility characteristics of the various polymer compounds, ligand exchange with ODA or OCA containing

polymers was carried out following slightly different protocols. For AMB-PIMA-ODA (**L1**) and IMB-PIMA-ODA (**L4**), the ligands are not soluble in polar media such as ethanol and methanol; the PQD stock dispersions in hexane were thus mixed with the polymer pre-dissolved in toluene yielding a clear mixture, then sonicated for ~5 minutes. The nanocrystals were washed with excess ethanol, precipitated, then re-dispersed in toluene and stored until further use. Conversely, the polymers containing short alkyl chains, AMB-PIMA-OCA (**L2**, **L3**) and IMB-PIMA-OCA (**L5**, **L6**) exhibit good solubility in ethanol and methanol. Ligand exchange and phase transfer was thus carried out using either a homogeneous one phase reaction (route 1), or a heterogeneous two-phase reaction (route 2), see **Figure 2A**. (1) In the one phase reaction, hydrophobic PQDs dispersed in hexane were mixed with a clear THF solution of the ligands **L2** and **L5** (containing 8 salt groups each) and sonicated for 3-5 minutes. The ligands containing 16 salt groups (i.e., **L3** and **L6**) were however not completely soluble in THF, but addition of EtOH (at ~EtOH:THF ~ 1:2) yielded a clear solution of those polymers. Mixing the OLA/OA-PQDs with either set of polysalts under these conditions allowed rapid ligand substitution, manifesting in a change in the nanocrystal solubility. This can be easily tested by adding excess hexane, which readily precipitates the PQDs, yielding a green pellet and a clear supernatant free of QD materials after centrifugation. After discarding the supernatant, the pellet was subjected to one or two more rounds of washing with ethyl acetate, then readily dispersed in EtOH or MeOH. (2) In the two-phase reaction (route 2), the nonpolar phase (hexane) containing OLA/OA-PQDs was mixed with a solution of the polysalt in methanol, yielding a top layer of hexane containing the PQDs and a bottom layer of the polymer solution in methanol. Sonication of the vial for 3-5 minutes readily promoted the transfer of the QDs to the methanol phase, as shown in **Figure 2A (R2)**. Decanting the hexane layer yielded a clear dispersion of the polymer-stabilized PQDs in methanol. While both methods effectively allow the phase transfer of the nanocrystals to polar solvents, each route offers a few advantages. For instance, route 1 minimizes exposure of the nanocrystals to polar conditions prior to complete ligand substitution with the polymer, and thus yields slightly more homogenous PQDs. Conversely, the bi-phasic reaction allows visual tracking of the phase transfer, but tends to produce traces of aggregated materials which result from transient exposure of the native QDs to methanol prior to a complete ligand substitution. Nonetheless, the small fraction of formed aggregates can be easily removed by centrifugation for 3-4 minutes, leaving a homogeneous dispersion of PQDs in methanol (see **Figure 2A**).

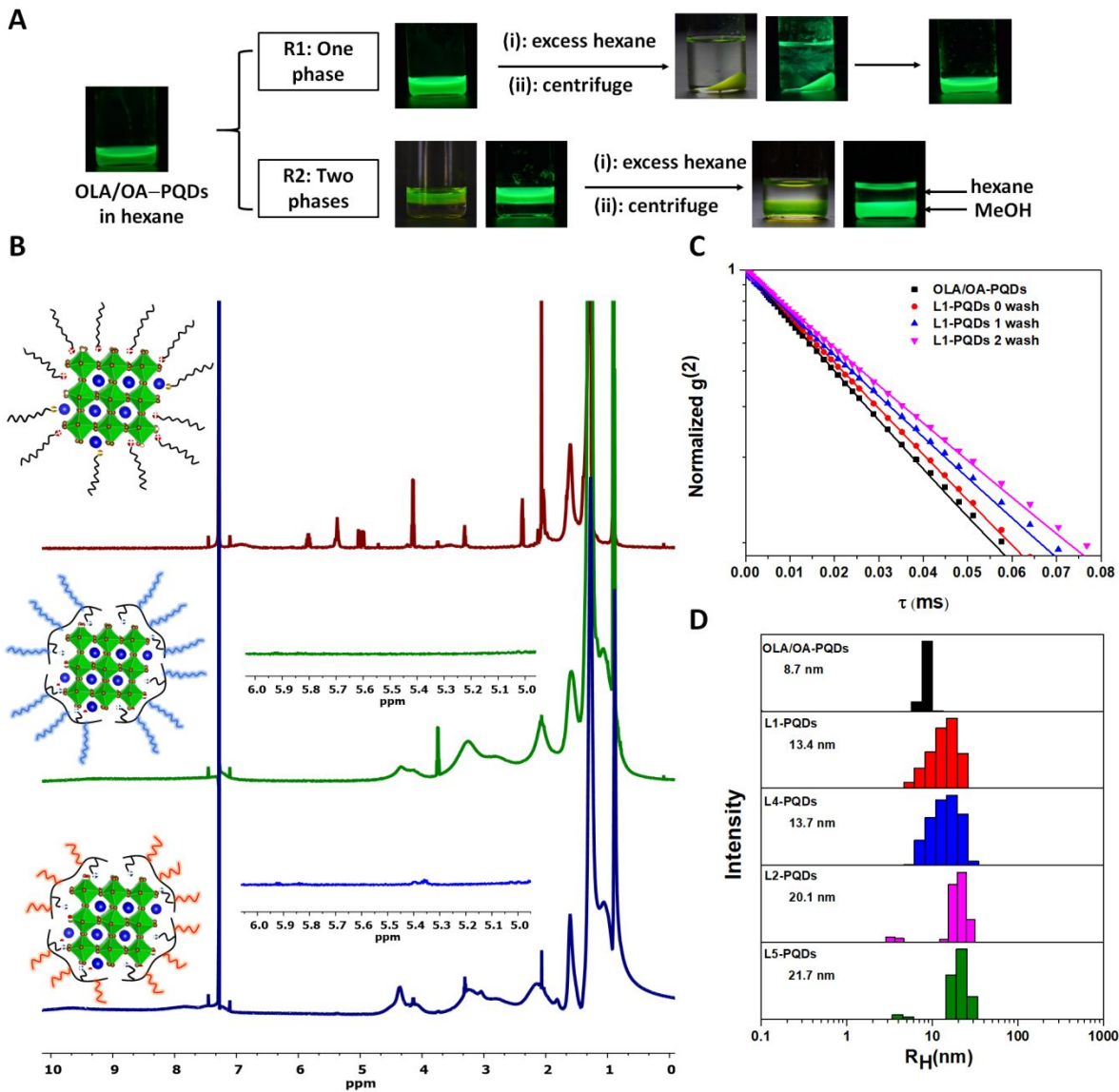


**Figure 2:** (A) Fluorescent images (generated using a hand-held UV lamp,  $\lambda_{exc} = 365$  nm) of PQRs collected during the ligand exchange steps with the polysalt ligands. One phase and two-phase routes are shown. (B)  $^1\text{H}$  NMR spectra of PQRs coated with OLA/OA, IMB-PIMA-ODA (**L4**) and IMB-PIMA-OCA (**L5**) ligands; the PQRs were dispersed in  $\text{CDCl}_3$ . (C) Semi-logarithmic plot of the normalized intensity autocorrelation function ( $g^{(2)}$ ) vs  $\tau$  recorded for PQR dispersions before, right after mixing with AMB-PIMA-ODA (**L1**) and after one time and two times washing with EtOH. (D) Histogram of hydrodynamic size distribution extracted from the Laplace transform of the autocorrelation functions built using the scattering data generated from the various PQR dispersions.

## Characterization of the Ligand Substitution Using NMR Spectroscopy and Dynamic Light Scattering

Effectiveness of the surface stabilization strategy is paramount to both extracting accurate data on how the new ligands affect the photophysical characteristics of the materials and for their potential integration into various devices. We characterized the completeness of the ligand substitution by tracking changes in the  $^1\text{H}$  NMR spectra collected from PQD dispersions after coating with the polysalts, compared to a typical spectrum collected from a dispersion of as-grown nanocrystals. **Figure 2B** shows a representative side-by-side comparison between the  $^1\text{H}$  NMR spectrum collected from OLA/OA-PQDs (top spectrum) and those measured from dispersions of nanocrystals stabilized with two IMB-based polysalt ligands, **L4**(IMB-PIMA-ODA)-PQDs and **L5**(IMB-PIMA-OCA)-PQDs, see middle and bottom spectra. The polymer-coated samples have been subjected to two rounds of purification then dispersed in  $\text{CDCl}_3$ , while the dispersions of native PQDs have been subjected to only one cycle. The spectrum of the native PQDs shows signatures ascribed to oleate and oleylammonium protons in the 3-6 ppm range, in particular the alkene peak at 5.37 ppm, which is in good agreement with previous reports.<sup>19-20, 50</sup> After ligand exchange with **L4** and **L5**, the spectra show several peaks spanning the range of 0-2 ppm, which are ascribed to the lateral alkyl chains and dimethyl protons along the PIMA backbone. Additionally, these spectra show broad peaks at  $\sim 4.3$  ppm, which can be ascribed to the two ethylene  $-\text{CH}_2-$  directly attached to the imidazolium ring ( $\text{N}_3$  position). Moreover, the characteristic downfield peaks of the imidazolium ring protons are not clearly discernable in both spectra, presumably due to signal reduction and peak broadening, which can be attributed to two factors: a drastically reduced segmental mobility of the surface-coordinated imidazolium groups and a rather poor ligand solvation in  $\text{CDCl}_3$ .<sup>53-54</sup> Despite the ambiguity caused by the pronounced signal overlap in the upfield region (where the alkyl signatures are), the absence of signatures in the 5-6 ppm provides a solid proof for the complete removal of the native ligands from the polysalt-stabilized PQD samples (compare top spectrum to the middle and bottom spectra).<sup>50</sup>

Another test focused on verifying that the polysalt coating provides ample steric stabilization to the PQD nanocolloids, in addition to enhancing PL. We applied dynamic light scattering (DLS) measurements to extract estimate of the hydrodynamic size and verify the homogeneity of the PQD colloidal dispersions. A plot of the autocorrelation function of the

scattered intensity,  $g^{(2)}(\theta, \tau)$  vs  $\tau$  (in semi-logarithmic scale) acquired from a dispersion of OLA/OA–PQDs shortly after mixing with excess IMB-PIMA-ODA (**L4**) shows that a slightly slower decay profile was acquired from the DLS data (see **Figure 2C**). This accounts for a slight reduction in the Brownian diffusion of the nanocolloids compared to OLA/OA–PQDs, and reflects that a rapid adsorption of the polymer ligands onto the NCs has taken place. Applying one or two rounds of washing with ethanol further reduced the decay slope of the nanocolloids, resulting from the complete removal of the native ligands and their substitution with the polysalt, until equilibrium conditions are reached. **Figure 2D** shows a set of intensity vs hydrodynamic size histograms measured for dispersions of OLA/OA– and AMB/IMB-PIMA-ODA–PQDs in toluene and AMB/IMB-PIMA-OCA–PQDs in EtOH; these were extracted from the Laplace Transform of  $g^{(2)}$  vs  $\tau$  profiles.<sup>55</sup> A single population is measured for all the samples, indicating that the PQD dispersions, before and after ligand substitution, are homogeneous and free of aggregates. Data also indicate that the smallest size was measured for the native coating,  $R_H \sim 8.7$  nm, then the size slightly increased to  $R_H$ (**L1**– and **L4**–PQDs in toluene)  $\sim 13$ -14 nm and  $R_H$ (**L2**– and **L5**–PQDs in EtOH)  $\sim 20$ -22 nm. These slight variations reflect differences in the hydrodynamic contributions of the coating to the Brownian diffusion of PQDs. More precisely, the larger size of the polysalts compared to the native OLA/OA yields higher contribution of the hydrodynamic interactions to the measured  $R_H$  compared to that measured for the as-grown materials.

### Optical Characterization

Having established the ability of the polysalts to rapidly promote ligand exchange and phase transfer of the PQDs, we proceeded to characterize the optical properties of the resulting materials. More precisely, we first compared side-by-side the absorption and photoluminescence spectra collected from the PQDs coated with the various AMB- and IMB-PIMA-OCA ligands (e.g., **L2** and **L5**) dispersed in EtOH to those measured for OLA/OA–PQDs in hexane, see **Figure 3A**. There is a close match between the absorption profiles of both sets of materials, clearly indicating a retention of the nanocrystal integrity after ligand substitution. The PL intensity of the polysalt-capped samples was enhanced by 1.5 times, compared to the starting PQDs. The corresponding average PL lifetimes, extracted for the time-resolved decay profiles shown in **Figure 3B**, are also longer than those measured for the as-grown materials, indicating reduction in the number of nonradiative channels (i.e. surface trap states) by the polysalt coating. Indeed, near-unity absolute

PLQY ( $\geq 95\%$ ) was measured for both AMB-PIMA-OCA (**L2**, **L3**)- and IMB-PIMA-OCA (**L5**, **L6**)-coated samples, compared to PLQY of  $\sim 65\%$  for OLA/OA-PQDs. Similar effects were also measured for the PQDs ligand substituted with AMB-PIMA-ODA and IMB-PIMA-ODA (**L1** and **L4**) and dispersed in toluene, namely fully preserved optical absorption and emission profiles and near unity PLQY were measured, see **Figure 3C-D**. The consistency of the results obtained for all polysalt (**L1** - **L6**)-stabilized CsPbBr<sub>3</sub> nanocrystals proves the importance of the salt groups for providing higher degree of surface passivation than OLA/OA and rules out potential additional effects of size or number of the solubilizing alkyl chains used. The lifetime data were compared to the changes in the ensemble fluorescence intensity using the relation for the PLQY:<sup>56</sup>

$$PLQY = \frac{k_r}{k_r + k_{nr}} \quad (1)$$

where  $k_r$  and  $k_{nr}$  respectively designate the radiative and nonradiative decay rates. Assuming that only  $k_{nr}$  is altered by electronic passivation of the surface traps, we compared the changes in the PLQY extracted from the ensemble PL to those extracted from changes in the lifetime data:

$$\frac{PL_{polysalt}}{PL_{native}} = \frac{PLQY_{polysalt}}{PLQY_{native}} = \frac{k_r - native + k_{nr - native}}{k_r - polysalt + k_{nr - polysalt}} = \frac{\tau_{polysalt}}{\tau_{native}} \quad (2)$$

where we replaced  $\frac{1}{k_r + k_{nr}}$  with the PL lifetime,  $\tau$ , extracted from the experimental data. From the steady-state and time-resolved data, estimates of the changes in the PLQY were compared to changes in the lifetime (see **Table 1**). Data show that the PLQY and lifetime before after ligand substitution are consistently higher than 1 for both sets of polysalts, implying that the ligands improve the fluorescence properties of the nanocrystals. Nonetheless, the ratios extracted for the PL were slightly higher than those deduced for the lifetime data. For example, for the IMB-presenting polysalt, we found:

$$\frac{PL_{polysalt - IMB}}{PL_{native}} \sim 1.62, \text{ or } 1.55 \quad \text{and} \quad \frac{\tau_{polysalt - IMB}}{\tau_{native}} \sim 1.27 \text{ or } 1.34 \quad (\text{for ODA and OCA}).$$

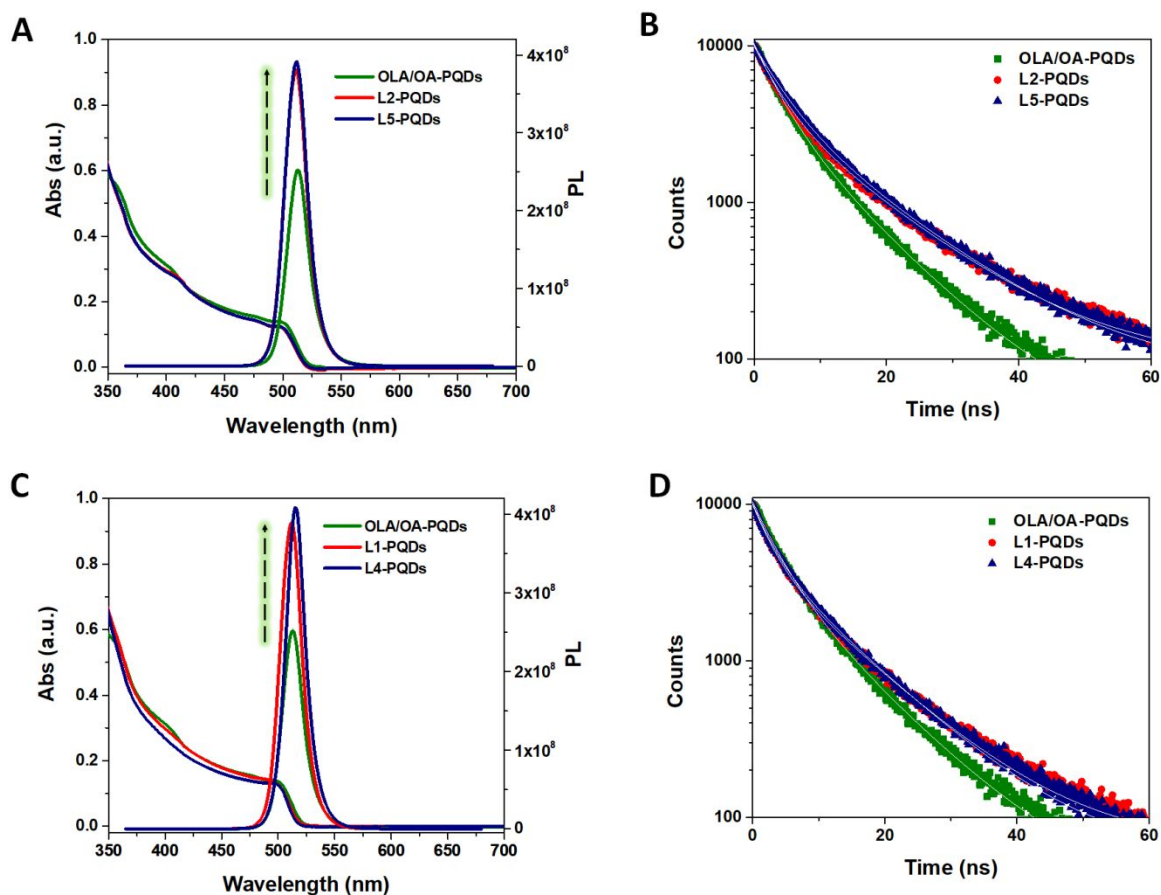


**Figure 3:** (A) Absorption and fluorescence spectra of OLA/OA–PQDs in hexane along with AMB-PIMA-ODA (L2)–PQDs and IMB-PIMA-ODA (L5)–PQDs dispersed in EtOH. (B) The time-resolved PL decay profiles of the three sets of PQDs shown in A. (C) Absorption and fluorescence spectra collected from dispersions of OLA/OA–PQDs in hexane, L1–PQDs and L4–PQDs dispersed in toluene. (D) The time-resolved PL decay profiles of the three sets of PQDs shown in C.

### Characterization of the Crystal Structure and Morphology of the PQD Colloids

We first carried out powder X-ray diffraction (PXRD) experiments to identify the crystalline structure of the PQDs before and after stabilization with the different polysalt coatings. **Figure 4A** shows the PXRD patterns acquired from the native OLA/OA–PQDs along with those ligand-exchanged with the set of polysalt ligands (L1, L2, L4, L5). Close inspection of the patterns reveals highly crystallized orthorhombic (Pnma) perovskite phase for all samples, confirmed by the close matching with the pattern measured for the bulk perovskite standard (ICSD number **243735**).<sup>57–59</sup> We note that in our previous report,<sup>50</sup> we fitted the PXRD patterns to a cubic structure. However, given the close patterns measured for the cubic and orthorhombic phases and recent

progress in the literature, we have now compared our XRD data to orthorhombic crystal structure.<sup>59</sup> The above result combined with absence of any “impurity peaks” from those spectra clearly indicate preserved crystal structure of the PQDs after ligand substitution with the polysalts. We then used high-angle-annular-dark-field scanning transmission electron microscopy (HAADF-STEM) to gain information about the spacing between the crystal planes, morphology and size distribution of the polysalt-stabilized PQDs, compared to the native OLA/OA-capped NCs. We focused on the TEM images acquired from nanocrystals ligated with **L2** (AMB20%-PIMA-OCA)

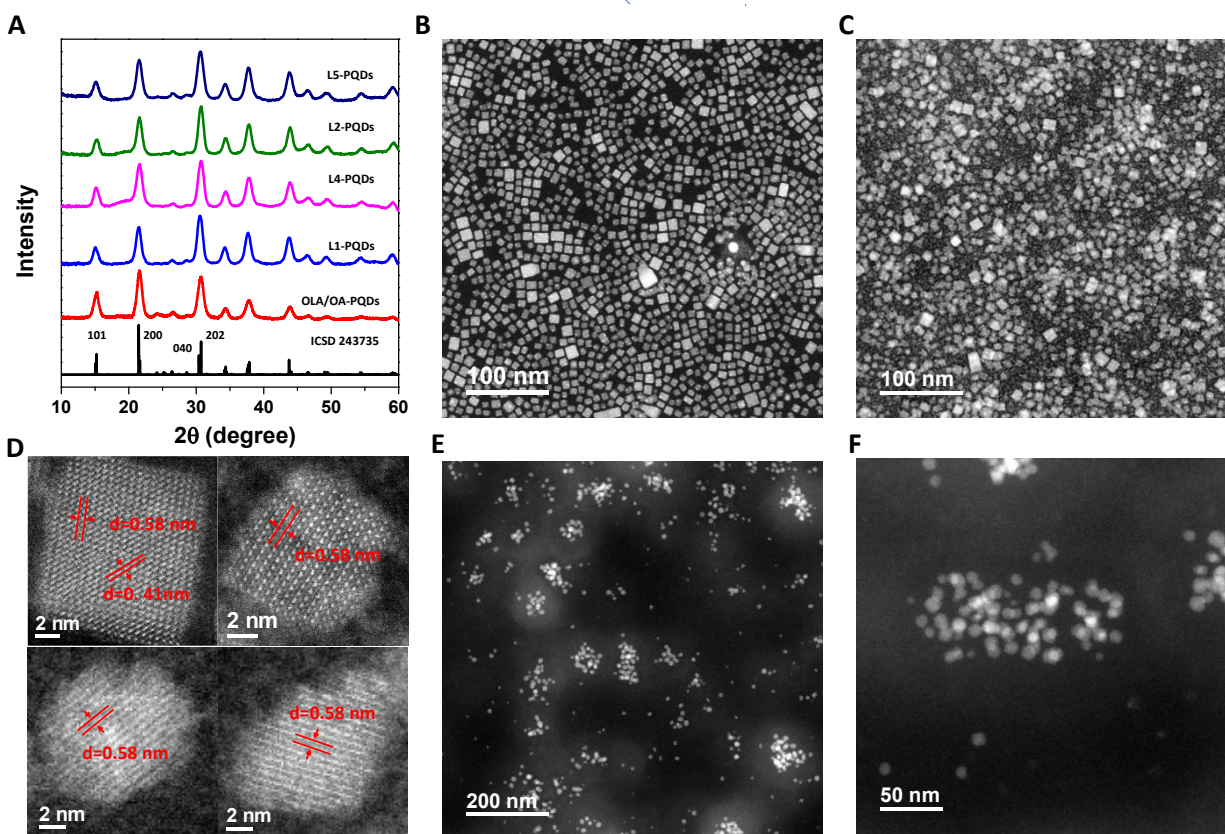


**Figure 4:** (A) Powder XRD patterns of the native PQDs along with nanocrystals ligand exchanged with various polysalts. (B,C) HAADF-STEM images of OLA/OA-PQDs and AMB20%-PIMA-OCA-PQDs (**L2**). (D) Representative high resolution TEM images of single perovskite nanocrystals acquired from: OLA/OA-PQDs (top left); **L2**(AMB20%-PIMA-OCA)-PQDs (top right); **L5**(IMB20%-PIMA-OCA)-PQDs (bottom left and bottom right). (E,F) Lower magnification HAADF-STEM images of **L5**(IMB20%-PIMA-OCA)-PQDs. All polysalt-coated PQDs have been aged in EtOH for ~3 months prior to TEM measurements.

and **L5** (IMB20%-PIMA-OCA) which allow phase transfer of PQDs to polar media, providing a more convincing proof that those polymers preserve the integrity of the nanocrystal characteristic features under polar solution conditions (namely, size, shape and crystal structure). In order to examine whether or not possible changes in the core shape and size can take place during long-term storage, **L2**- and **L5**-stabilized PQDs dispersed in EtOH were first aged for ~3 months, then HAADF-STEM images were acquired. Freshly prepared OLA/OA-PQDs with cuboidal shape, sharp edges, and an average cube side length of ~7.2 nm were used as a reference, see **Figure 4, panel B**. The image shown in **Figure 4, panel C** indicates that **L2**-stabilized PQDs prepared from dispersion in EtOH maintained their cubic shape with an average side length of ~7.4 nm. This proves that following ligand substitution the NPs preserve their overall size, shape, and stay homogenous and free of aggregates, albeit with a slightly broader size distribution (compare **Figures 4B** and **4C**). Nonetheless, PQDs ligand exchanged with **L5** (IMB20%-PIMA-OCA) exhibited more pronounced changes in size and morphology. Though a cuboidal shape for the **L5**-PQDs can still be identified in the TEM image, a loss of corner sharpness and occasional etching of the nanocrystals can be observed at higher magnification of individual nanocrystals (see **Figure 4D, bottom images**). An average side ~7.5 nm was measured for these nanocrystals. Additional histograms on the PQD size distribution for the characterized samples are provided in the **ESI, Figure S4**. Cumulatively, the data show that essentially small to negligible changes in the core size are noted for the polymer-coated PQDs, indicating that minimal morphological transformation of the nanocrystals has taken place. The TEM images acquired from all three sets of samples show high core crystallinity with well-resolved atomic arrangements, where the spacing between the (101) crystal planes is ~0.58 nm and that between the (200) planes is ~0.41 nm (see panel 4A). Additionally, the images of **L2**-PQDs show that the nanocrystals have preserved their cubic morphology in agreement with the starting OLA/OA-PQDs, but showed partial loss in the definition of the cube edges/corners. Conversely, the TEM images of **L5**-PQDs showed more visible corner etching, which can be identified under crystal orientation (see **Figure 4D, bottom images**).<sup>60-61</sup> Interestingly, the PLQY measured for dispersion of all PQD samples after ligand substitution remained high. These findings indicate that the etching observed for some of the nanocrystal surfaces do not negatively affect the fluorescence properties of the materials. We attribute this to a more effective passivation of the surface defects brought by the multi-

coordination of the nanocrystals after ligand substitution. This reduced the overall rate of non-radiative exciton recombination for these dispersions.

Finally, we would like to note that even though the TEM images show rather homogeneously distributed nanocrystals on the grid for OLA/OA–PQDs and **L2**–PQDs, the images collected from the **L5**–PQDs indicate that some degree of nanocrystal clustering, within discrete regions, builds up during the drying process, see low magnification images in **Figure 4E&F** and **Figure S5**. We attribute this to inhomogeneous drying of the polymer-ligated PQDs on the TEM grid, a process likely due to the nature of the IMB-PIMA-OCA ligand and its affinity to EtOH.

### Stability Tests

Having demonstrated that ligand exchange of the nanocrystals with the different polysalts is rapid and efficient, we proceeded to evaluate the colloidal stability of the surface-modified PQDs under a few relevant test conditions.

1- We first implemented the ubiquitous polar solvent wash test (e.g., ethanol or ethyl acetate). This method has been widely used for testing the new ligand affinity to the PQDs.<sup>21, 26, 30</sup> Additionally, washing with a polar solvent is a common technique for removing free OLA/OA ligands from the medium, which is critical for integration into optoelectronic devices and improving the device efficiency.<sup>35, 38</sup> Here, we compared the behaviors of OLA/OA–PQDs and polysalt–PQDs subjected to such treatment. We found that one wash of OLA/OA–PQDs with ethanol promoted a rapid formation of a yellowish macroscopic aggregate and pronounced loss of emission, as shown in **Figure 5A**. In contrast, dispersions of PQDs stabilized with **L1**(AMB-PIMA-ODA) or with **L4**(IMB-PIMA-ODA) preserved their colloidal integrity and strong emission properties, even when subjected to as many as five rounds of washing with ethanol, as reflected by the clear green fluorescent dispersions shown in **Figure 5A**. Interestingly, the graph shown in **Figure 5B** indicates that the effects of implementing the ligand substitution on the PL changes are subtle. Following a simple mixing of a dispersion of OLA/OA–PQDs with the polysalt yielded a modest increase in the PL intensity (~30%). However, applying one round of washing with ethanol produced a large PL increase (~80%); further washing with ethanol did not affect the PL increase. We attribute this result to the removal of the native OLA/OA ligands and the ability of the polysalts to repair defects sites, passivate energy traps and improve the materials colloidal stability.

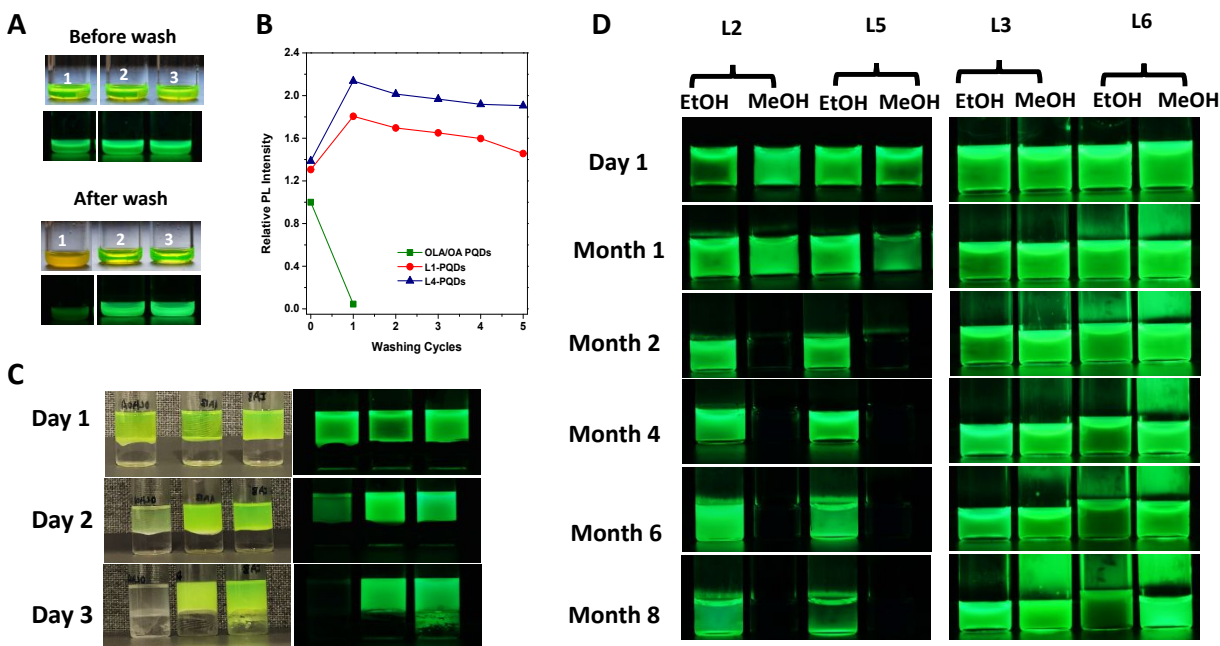


**Figure 5:** (A) White light and fluorescence images acquired from dispersions of the native PQDs (1) before and after one EtOH wash, along with dispersions of L1-PQDs (2) and L4-PQDs (3), before and after 5 rounds of EtOH wash. (B) Plot of the relative PL intensity measured for pristine OLA/OA-PQDs, or L1-PQDs and L4-PQDs subjected to different EtOH wash cycles. (C) White light and fluorescence images acquired from OLA/OA-, L1- and L4-PQDs taken during the water resistance test; top layer is toluene and bottom layer is DI water. (D) Fluorescence images of AAB-PIMA-OCA (L2 and L3)- and IAB-PIMA-OCA (L5 and L6)-PQDs dispersions in EtOH and MeOH tracked during storage for 8-months.

2- We then evaluated the resistance of PQDs to water-induced degradation for the three sets of samples, OLA/OA-PQDs, L1- and L4-stabilized PQDs, using a two-phase (organic/water) configuration.<sup>62</sup> As shown in **Figure 5C**, two separate phases are formed after mixing the dispersions with water, with the top toluene phase containing the PQDs and DI water in the bottom phase, due to the immiscible nature of the two liquids. Nonetheless, interaction between the PQDs and water can still take place through the interfacial interactions at the meniscus, in part due to local mixing and non-negligible water dissolution in toluene; water solubility in toluene at ambient conditions is at  $\sim 0.027$  M.<sup>63</sup> This caused turbidity buildup in the OLA/OA-PQDs layer combined with loss of fluorescence emission after one day, as shown in the white light and fluorescence images collected from these nanocrystal dispersions. In contrast, L1- and L4-stabilized PQDs stayed dispersed and strongly fluorescent over the 3-day test period.

3- We carried out long-term colloidal stability tests, which is a highly relevant criterion for evaluating the effectiveness of the polysalt ligands to coordinate and stabilize the nanocrystals in solution. We probed the homogeneity and PL stability of PQDs ligand substituted with **L2** and **L5**, or **L3** and **L6**, and dispersed in two polar protic alcohols (EtOH and MeOH). **Figure 5D, left panel** shows the fluorescence images of PQDs dispersions freshly prepared and after several months of storage under room light and temperature conditions. The PQDs coated with **L2** or **L5** (presenting 8 AMB or 8 IMB groups per ligand) exhibit rather limited stability in MeOH, where aggregation and PL quenching occurred after 1 month of storage. Better stability is shown in ethanol where homogeneity of the dispersion and high fluorescence emission are preserved for at least 4 months. In comparison, the colloidal and photophysical stability are much improved for PQDs that have been coated with ligands that present ~16 salt groups per chain (i.e., **L3** and **L6**). As shown in **Figure 5D, panel 2**, the 4 PQD samples stayed homogenous and highly fluorescent after 8 months of storage, a result that can be attributed to the stronger ligand affinity to the PQDs. Additionally, the absolute PLQY measured for the PQD dispersions in EtOH stayed above 90% for at least three months (**Figure S6**). These findings agree with the reported benefits of using multi-coordinating ligands to impart long term structural and photophysical stability onto plasmonic and conventional luminescent nanocolloid materials.<sup>64-65</sup> Nonetheless, there are some subtle differences between ligands appended with ammonium and imidazolium salt groups. In general, we found that AMB-based polymers (e.g., **L2** and **L3**) impart better stability to NCs, which may likely be due to the smaller alkyl ammonium anchors compared to imidazolium rings. **Figure 5D** and **Figure S7** show that **L2**-PQDs in ethanol maintain colloidal homogeneity and high PL for up to 6 months, while **L3**-PQDs stay stable for over one year of storage. This can be contrasted with IMB-PIMA-OCA-PQDs, which lose their colloidal stability and/or emission properties after ~4 months for **L5** and after ~8 months for **L6**.

We now discuss our findings in comparison to previous literature data and provide a few insights into how the polysalts combine strong coordination interactions and electronic passivation of the PQD surfaces. In particular, our comparison will focus on data collected from either treating the as grown CsPbBr<sub>3</sub> QDs with the molecular scale quaternary ammonium bromide, DDAB, or ligand substitution of the nanocrystals with these and other coordinating molecules. Those studies have overall reported that DDAB and other bromide salts can improve the photoemission

properties of PQDs.<sup>13, 22, 25</sup> Nonetheless, monomer ligands applied to any colloidal nanocrystals tend to exhibit rather high rates of desorption due to the nature of coordination interactions.<sup>66</sup>

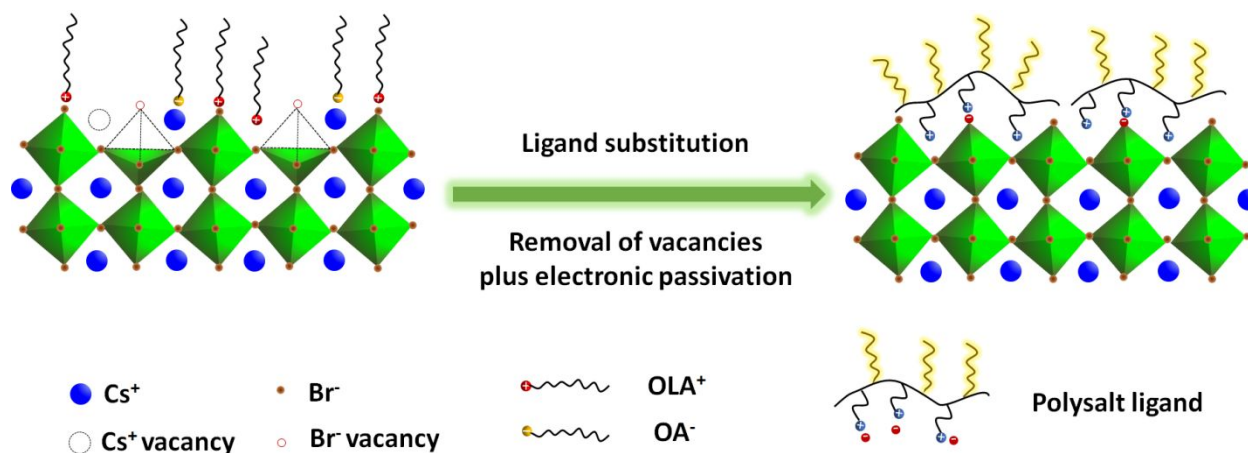


**Figure 6:** Schematic representation of the benefits combining bromide vacancy filling and electrostatic passivation of the Cs<sup>+</sup> sites provided by the multidentate polysalt ligand coating, yielding enhanced PL and long-term colloidal stabilization of the PQDs.

Our ligand design strategy to install several quaternary ammonium or imidazolium groups along a polymer backbone has promoted a substantial reduction in the rate of desorption, resulting in strengthened ligand interactions with the PQDs. This enabled a more efficient elimination of bromide vacancies ( $V_{\text{Br}}$ ), better passivation of the Pb<sup>2+</sup> sites, and filling the Cs<sup>+</sup> vacancies, thus restoring damaged lead-bromide octahedra near the NC surface (see **Figure 6**). This has also improved the rate of exciton radiative recombination, ultimately increasing the measured PLQY to near unity, which is in agreement with data collected using monomeric DDAB.<sup>22, 67</sup> Furthermore, multi-coordinating polymer ligands containing either ammonium or imidazolium cations would have more stable binding to the surface bromide ions, while promoting steric repulsions between individual PQDs brought by the multi-alkyl chains, compared to the monodentate DDAB ligands. This ultimately resulted in enhanced colloidal stability. We should also note that though some degree of surface etching of the NCs has been observed when using imidazolium-presenting polysalts, the absorption and PL spectra measured for those PQDs were unaffected. This indicates that slight damage of the nanocrystal surface does not significantly affect the photophysics of these materials, given their reported high tolerance to defects.<sup>2, 17</sup> Finally, we would like to compare the present coating strategy results to those using polyzwitterionic ligands, described in references.<sup>50,</sup>

<sup>68-69</sup> The two sets of ligands (polyzwitterion and polysalt) interact differently with the NC surfaces. While the polysalts can restore surface vacancies and removal of energy traps, their binding interaction are weaker than those afforded by the zwitterion-rich ligands. Polymer ligands based on the zwitterion motif(s) present two complementary coordinating groups (Lewis base and Lewis acid) which allow interactions with anionic and cationic sites on the PQDs, while a polysalt has only one set. This explains the better long term colloidal stability afforded by sulfobetaine-rich polymers such as those investigated in reference.<sup>50</sup>

## Conclusion

We have designed and tested a set of polysalt compounds that combine several quaternary ammonium- or imidazolium salt groups with multiple alkyl chains as high affinity coordinating ligands that promote colloidal stabilization while increasing the photoluminescence quantum yield of CsPbBr<sub>3</sub> PQDs. The salt groups and solubilizing alkyl chains were installed along a low molecular weight anhydride-rich copolymer using the nucleophilic addition reaction. We found that these polysalts provide rapid ligand substitution of the native coating, enhance the colloidal stability under various conditions (including extended storage in polar solutions, repeated washes with anti-solvents and exposure to water) and increase the PLQY to near unity, all without altering the crystalline structure or morphology of the nanocrystals. Complete removal of the native coating was confirmed using NMR spectroscopy.

We attribute the effectiveness of these ligands to the strong coordination interactions of the polysalts with the QD surfaces, and the ability of the ammonium or imidazolium bromide salt groups to provide two important features: 1) repairing of surface defect sites, by sharing the bromide anions with the nanocrystal surfaces; 2) filling the empty Cs<sup>+</sup> site with quaternary ammonium or imidazolium cations. These provide efficient electronic passivation of the surface energy traps, and in turn increase the exciton radiative recombination rate and enhance the PLQY of the dispersions to near unity. These results confirm the importance of combining high coordination with the specific salt structure for achieving increased ligand affinity to the nanocrystals while drastically reducing the rates of ligand desorption. This design could be used to develop other polysalt compounds that can be used with other perovskite core stoichiometry. We are presently investigating the ability of these ligands to surface passivate and stabilize anisotropic CsPbBr<sub>3</sub> 2D nanoplates, where we measured improved PLQY and stability. We hope to report on these findings in the future. Other potential use of these rationales could involve the synthesis of other halide (chloride or iodide) polysalts to promote better passivation of other core perovskite materials. Indeed, electronic passivation and structural stabilization of such materials is critical for further integration of these materials in variety of optoelectronic applications.<sup>70</sup>

### **Electronic Supplementary Information**

Additional information, Materials, Instrumentation, NMR spectra of several polysalt ligands, TEM data of certain polysalt–QDs, and colloidal stability tests. This information is available free of charge on the RSC Publications website.

### **Conflicts of interest**

There are no conflicts of interest to declare

### **Acknowledgments**

The authors thank FSU and the National Science Foundation (NSF-CHE, Grants #1508501 and #2005079), AFOSR (Grant No. FA9550-18-1-0144) and Kasei-Asahi Corporation for financial support. TEM experiments were performed at the National High Magnetic Field Laboratory, which is supported by National Science Foundation Cooperative Agreement No. DMR-1644779 and the State of Florida (Grant No. FA9550-18-1-0144).

## REFERENCES

1. Akkerman, Q. A.; Rainò, G.; Kovalenko, M. V.; Manna, L., Genesis, challenges and opportunities for colloidal lead halide perovskite nanocrystals. *Nat. Mater.* **2018**, *17*, 394-405.
2. Kovalenko, M. V.; Protesescu, L.; Bodnarchuk, M. I., Properties and potential optoelectronic applications of lead halide perovskite nanocrystals. *Science* **2017**, *358*, 745-750.
3. Almeida, G.; Infante, I.; Manna, L., Resurfacing halide perovskite nanocrystals. *Science* **2019**, *364*, 833-834.
4. Shamsi, J.; Urban, A. S.; Imran, M.; De Trizio, L.; Manna, L., Metal Halide Perovskite Nanocrystals: Synthesis, Post-Synthesis Modifications, and Their Optical Properties. *Chem. Rev.* **2019**, *119*, 3296-3348.
5. Protesescu, L.; Yakunin, S.; Bodnarchuk, M. I.; Krieg, F.; Caputo, R.; Hendon, C. H.; Yang, R. X.; Walsh, A.; Kovalenko, M. V., Nanocrystals of Cesium Lead Halide Perovskites (CsPbX<sub>3</sub>, X = Cl, Br, and I): Novel Optoelectronic Materials Showing Bright Emission with Wide Color Gamut. *Nano Lett.* **2015**, *15*, 3692-3696.
6. Wei, S.; Yang, Y.; Kang, X.; Wang, L.; Huang, L.; Pan, D., Room-temperature and gram-scale synthesis of CsPbX<sub>3</sub> (X = Cl, Br, I) perovskite nanocrystals with 50–85% photoluminescence quantum yields. *Chem. Commun.* **2016**, *52*, 7265-7268.
7. Sanehira, E. M.; Marshall, A. R.; Christians, J. A.; Harvey, S. P.; Ciesielski, P. N.; Wheeler, L. M.; Schulz, P.; Lin, L. Y.; Beard, M. C.; Luther, J. M., Enhanced mobility CsPbI<sub>3</sub> quantum dot arrays for record-efficiency, high-voltage photovoltaic cells. *Sci. Adv.* **2017**, *3*, eaao4204.
8. Fu, H., Colloidal metal halide perovskite nanocrystals: a promising juggernaut in photovoltaic applications. *J. Mater. Chem. A* **2019**, *7*, 14357-14379.
9. Swarnkar, A.; Marshall, A. R.; Sanehira, E. M.; Chernomordik, B. D.; Moore, D. T.; Christians, J. A.; Chakrabarti, T.; Luther, J. M., Quantum dot-induced phase stabilization of  $\alpha$ -CsPbI<sub>3</sub> perovskite for high-efficiency photovoltaics. *Science* **2016**, *354*, 92-95.
10. Jeong, M.; Choi, I. W.; Go, E. M.; Cho, Y.; Kim, M.; Lee, B.; Jeong, S.; Jo, Y.; Choi, H. W.; Lee, J.; Bae, J.-H.; Kwak, S. K.; Kim, D. S.; Yang, C., Stable perovskite solar cells with efficiency exceeding 24.8% and 0.3-V voltage loss. *Science* **2020**, *369*, 1615-1620.
11. Chiba, T.; Kido, J., Lead halide perovskite quantum dots for light-emitting devices. *J. Mater. Chem. C* **2018**, *6*, 11868-11877.
12. Lu, M.; Zhang, Y.; Wang, S.; Guo, J.; Yu, W. W.; Rogach, A. L., Metal Halide Perovskite Light-Emitting Devices: Promising Technology for Next-Generation Displays. *Adv. Funct. Mater.* **2019**, *29*, 1902008.
13. Pan, J.; Quan, L. N.; Zhao, Y.; Peng, W.; Murali, B.; Sarmah, S. P.; Yuan, M.; Sinatra, L.; Alyami, N. M.; Liu, J. et al., Highly Efficient Perovskite-Quantum-Dot Light-Emitting Diodes by Surface Engineering. *Adv. Mater.* **2016**, *28*, 8718-8725.
14. Yoon, H. C.; Lee, H.; Kang, H.; Oh, J. H.; Do, Y. R., Highly efficient wide-color-gamut QD-emissive LCDs using red and green perovskite core/shell QDs. *J. Mater. Chem. C* **2018**, *6*, 13023-13033.
15. Wang, Y.; Song, L.; Chen, Y.; Huang, W., Emerging New-Generation Photodetectors Based on Low-Dimensional Halide Perovskites. *ACS Photonics* **2020**, *7*, 10-28.

16. Chen, Q.; Wu, J.; Ou, X.; Huang, B.; Almutlaq, J.; Zhumekenov, A. A.; Guan, X.; Han, S.; Liang, L.; Yi, Z.; Li, J. et al., All-inorganic perovskite nanocrystal scintillators. *Nature* **2018**, *561*, 88-93.
17. Huang, H.; Bodnarchuk, M. I.; Kershaw, S. V.; Kovalenko, M. V.; Rogach, A. L., Lead Halide Perovskite Nanocrystals in the Research Spotlight: Stability and Defect Tolerance. *ACS Energy Lett.* **2017**, *2*, 2071-2083.
18. Ravi, V. K.; Santra, P. K.; Joshi, N.; Chugh, J.; Singh, S. K.; Rensmo, H.; Ghosh, P.; Nag, A., Origin of the Substitution Mechanism for the Binding of Organic Ligands on the Surface of CsPbBr<sub>3</sub> Perovskite Nanocubes. *J. Phys. Chem. Lett.* **2017**, *8*, 4988-4994.
19. De Roo, J.; Ibáñez, M.; Geiregat, P.; Nedelcu, G.; Walravens, W.; Maes, J.; Martins, J. C.; Van Driessche, I.; Kovalenko, M. V.; Hens, Z., Highly Dynamic Ligand Binding and Light Absorption Coefficient of Cesium Lead Bromide Perovskite Nanocrystals. *ACS Nano* **2016**, *10*, 2071-2081.
20. Smock, S. R.; Williams, T. J.; Brutchey, R. L., Quantifying the Thermodynamics of Ligand Binding to CsPbBr<sub>3</sub> Quantum Dots. *Angew. Chem. Int. Ed.* **2018**, *57*, 11711-11715.
21. Bodnarchuk, M. I.; Boehme, S. C.; ten Brinck, S.; Bernasconi, C.; Shynkarenko, Y.; Krieg, F.; Widmer, R.; Aeschlimann, B.; Günther, D.; Kovalenko, M. V.; Infante, I., Rationalizing and Controlling the Surface Structure and Electronic Passivation of Cesium Lead Halide Nanocrystals. *ACS Energy Lett.* **2019**, *4*, 63-74.
22. Imran, M.; Ijaz, P.; Goldoni, L.; Maggioni, D.; Petralanda, U.; Prato, M.; Almeida, G.; Infante, I.; Manna, L., Simultaneous Cationic and Anionic Ligand Exchange For Colloidally Stable CsPbBr<sub>3</sub> Nanocrystals. *ACS Energy Lett.* **2019**, *4*, 819-824.
23. Dong, Y.; Wang, Y.-K.; Yuan, F.; Johnston, A.; Liu, Y.; Ma, D.; Choi, M.-J.; Chen, B.; Chekini, M.; Baek, S.-W. et al., Bipolar-shell resurfacing for blue LEDs based on strongly confined perovskite quantum dots. *Nat. Nanotechnol.* **2020**, *15*, 668-674.
24. Owen, J., The coordination chemistry of nanocrystal surfaces. *Science* **2015**, *347*, 615-616.
25. Ye, J.; Byranvand, M. M.; Martínez, C. O.; Hoye, R. L. Z.; Saliba, M.; Polavarapu, L., Defect Passivation in Lead-Halide Perovskite Nanocrystals and Thin Films: Toward Efficient LEDs and Solar cells. *Angew. Chem. Int. Ed.* **2021** ASAP. doi.org/10.1002/anie.202102360.
26. Krieg, F.; Ochsenbein, S. T.; Yakunin, S.; ten Brinck, S.; Aellen, P.; Süess, A.; Clerc, B.; Guggisberg, D.; Nazarenko, O.; Shynkarenko, Y. et al., Colloidal CsPbX<sub>3</sub> (X = Cl, Br, I) Nanocrystals 2.0: Zwitterionic Capping Ligands for Improved Durability and Stability. *ACS Energy Lett.* **2018**, *3*, 641-646.
27. Krieg, F.; Ong, Q. K.; Burian, M.; Rainò, G.; Naumenko, D.; Amenitsch, H.; Süess, A.; Grotevent, M. J.; Krumeich, F. et al., Stable Ultraconcentrated and Ultradilute Colloids of CsPbX<sub>3</sub> (X = Cl, Br) Nanocrystals Using Natural Lecithin as a Capping Ligand. *J. Am. Chem. Soc.* **2019**, *141*, 19839-19849.
28. Zhang, B.; Goldoni, L.; Lambruschini, C.; Moni, L.; Imran, M.; Pianetti, A.; Pinchetti, V.; Brovelli, S.; De Trizio, L.; Manna, L., Stable and Size Tunable CsPbBr<sub>3</sub> Nanocrystals Synthesized with Oleylphosphonic Acid. *Nano Lett.* **2020**, *20*, 8847-8853.
29. Zhang, B.; Goldoni, L.; Zito, J.; Dang, Z.; Almeida, G.; Zaccaria, F.; de Wit, J.; Infante, I.; De Trizio, L.; Manna, L., Alkyl Phosphonic Acids Deliver CsPbBr<sub>3</sub> Nanocrystals with High Photoluminescence Quantum Yield and Truncated Octahedron Shape. *Chem. Mater.* **2019**, *31*, 9140-9147.
30. Tan, Y.; Zou, Y.; Wu, L.; Huang, Q.; Yang, D.; Chen, M.; Ban, M.; Wu, C.; Wu, T.; Bai, S., Highly Luminescent and Stable Perovskite Nanocrystals with Octylphosphonic Acid as a Ligand for Efficient Light-Emitting Diodes. *ACS Appl. Mater. Interfaces* **2018**, *10*, 3784-3792.

31. Yang, D.; Li, X.; Zhou, W.; Zhang, S.; Meng, C.; Wu, Y.; Wang, Y.; Zeng, H., CsPbBr<sub>3</sub> Quantum Dots 2.0: Benzenesulfonic Acid Equivalent Ligand Awakens Complete Purification. *Adv. Mater.* **2019**, *31*, 1900767.
32. Koscher, B. A.; Swabeck, J. K.; Bronstein, N. D.; Alivisatos, A. P., Essentially Trap-Free CsPbBr<sub>3</sub> Colloidal Nanocrystals by Postsynthetic Thiocyanate Surface Treatment. *J. Am. Chem. Soc.* **2017**, *139*, 6566-6569.
33. Nenon, D. P.; Pressler, K.; Kang, J.; Koscher, B. A.; Olshansky, J. H.; Osowiecki, W. T.; Koc, M. A.; Wang, L.-W.; Alivisatos, A. P., Design Principles for Trap-Free CsPbX<sub>3</sub> Nanocrystals: Enumerating and Eliminating Surface Halide Vacancies with Softer Lewis Bases. *J. Am. Chem. Soc.* **2018**, *140*, 17760-17772.
34. Ahmed, T.; Seth, S.; Samanta, A., Boosting the Photoluminescence of CsPbX<sub>3</sub> (X = Cl, Br, I) Perovskite Nanocrystals Covering a Wide Wavelength Range by Postsynthetic Treatment with Tetrafluoroborate Salts. *Chem. Mater.* **2018**, *30*, 3633-3637.
35. Hoshi, K.; Chiba, T.; Sato, J.; Hayashi, Y.; Takahashi, Y.; Ebe, H.; Ohisa, S.; Kido, J., Purification of Perovskite Quantum Dots Using Low-Dielectric-Constant Washing Solvent "Diglyme" for Highly Efficient Light-Emitting Devices. *ACS Appl. Mater. Interfaces* **2018**, *10*, 24607-24612.
36. Wu, H.; Zhang, Y.; Lu, M.; Zhang, X.; Sun, C.; Zhang, T.; Colvin, V. L.; Yu, W. W., Surface ligand modification of cesium lead bromide nanocrystals for improved light-emitting performance. *Nanoscale* **2018**, *10*, 4173-4178.
37. Song, J.; Li, J.; Xu, L.; Li, J.; Zhang, F.; Han, B.; Shan, Q.; Zeng, H., Room-Temperature Triple-Ligand Surface Engineering Synergistically Boosts Ink Stability, Recombination Dynamics, and Charge Injection toward EQE-11.6% Perovskite QLEDs. *Adv. Mater.* **2018**, *30*, 1800764.
38. Chiba, T.; Hoshi, K.; Pu, Y.-J.; Takeda, Y.; Hayashi, Y.; Ohisa, S.; Kawata, S.; Kido, J., High-Efficiency Perovskite Quantum-Dot Light-Emitting Devices by Effective Washing Process and Interfacial Energy Level Alignment. *ACS Appl. Mater. Interfaces* **2017**, *9*, 18054-18060.
39. Park, J. H.; Lee, A.-y.; Yu, J. C.; Nam, Y. S.; Choi, Y.; Park, J.; Song, M. H., Surface Ligand Engineering for Efficient Perovskite Nanocrystal-Based Light-Emitting Diodes. *ACS Appl. Mater. Interfaces* **2019**, *11*, 8428-8435.
40. Moyon, E.; Jun, H.; Kim, H.-M.; Jang, J., Surface Engineering of Room Temperature-Grown Inorganic Perovskite Quantum Dots for Highly Efficient Inverted Light-Emitting Diodes. *ACS Appl. Mater. Interfaces* **2018**, *10*, 42647-42656.
41. Shin, Y. S.; Yoon, Y. J.; Lee, K. T.; Jeong, J.; Park, S. Y.; Kim, G.-H.; Kim, J. Y., Vivid and Fully Saturated Blue Light-Emitting Diodes Based on Ligand-Modified Halide Perovskite Nanocrystals. *ACS Appl. Mater. Interfaces* **2019**, *11*, 23401-23409.
42. Shynkarenko, Y.; Bodnarchuk, M. I.; Bernasconi, C.; Berezovska, Y.; Verteletskyi, V.; Ochsenbein, S. T.; Kovalenko, M. V., Direct Synthesis of Quaternary Alkylammonium-Capped Perovskite Nanocrystals for Efficient Blue and Green Light-Emitting Diodes. *ACS Energy Lett.* **2019**, *4*, 2703-2711.
43. Zhang, C.; Wang, B.; Wan, Q.; Kong, L.; Zheng, W.; Li, Z.; Li, L., Critical role of metal ions in surface engineering toward brightly luminescent and stable cesium lead bromide perovskite quantum dots. *Nanoscale* **2019**, *11*, 2602-2607.

44. Ruan, L. J.; Tang, B.; Ma, Y., Improving the Stability of CsPbBr<sub>3</sub> Nanocrystals in Ethanol by Capping with PbBr<sub>2</sub>-Adlayers. *J. Phys. Chem. C* **2019**, *123*, 11959-11967.
45. Pan, J.; Sarmah, S. P.; Murali, B.; Dursun, I.; Peng, W.; Parida, M. R.; Liu, J.; Sinatra, L.; Alyami, N.; Zhao, C. et al. , Air-Stable Surface-Passivated Perovskite Quantum Dots for Ultra-Robust, Single- and Two-Photon-Induced Amplified Spontaneous Emission. *J. Phys. Chem. Lett.* **2015**, *6*, 5027-5033.
46. Chiba, T.; Takahashi, Y.; Sato, J.; Ishikawa, S.; Ebe, H.; Tamura, K.; Ohisa, S.; Kido, J., Surface Crystal Growth of Perovskite Nanocrystals via Postsynthetic Lead(II) Bromide Treatment to Increase the Colloidal Stability and Efficiency of Light-Emitting Devices. *ACS Appl. Mater. Interfaces* **2020**, *12*, 45574-45581.
47. Wang, W.; Ji, X.; Kapur, A.; Zhang, C.; Mattoussi, H., A Multifunctional Polymer Combining the Imidazole and Zwitterion Motifs as a Biocompatible Compact Coating for Quantum Dots. *J. Am. Chem. Soc.* **2015**, *137*, 14158-14172.
48. Du, L.; Wang, W.; Zhang, C.; Jin, Z.; Palui, G.; Mattoussi, H., A Versatile Coordinating Ligand for Coating Semiconductor, Metal, and Metal Oxide Nanocrystals. *Chem. Mater.* **2018**, *30*, 7269-7279.
49. Wang, W.; Kapur, A.; Ji, X.; Safi, M.; Palui, G.; Palomo, V.; Dawson, P. E.; Mattoussi, H., Photoligation of an Amphiphilic Polymer with Mixed Coordination Provides Compact and Reactive Quantum Dots. *J. Am. Chem. Soc.* **2015**, *137*, 5438-5451.
50. Wang, S.; Du, L.; Jin, Z.; Xin, Y.; Mattoussi, H., Enhanced Stabilization and Easy Phase Transfer of CsPbBr<sub>3</sub> Perovskite Quantum Dots Promoted by High-Affinity Polyzwitterionic Ligands. *J. Am. Chem. Soc.* **2020**, *142*, 12669-12680.
51. Wang, W.; van Niekerk, E. A.; Zhang, Y.; Du, L.; Ji, X.; Wang, S.; Baker, J. D.; Groeniger, K.; Raymo, F. M.; Mattoussi, H., Compact, "Clickable" Quantum Dots Photoligated with Multifunctional Zwitterionic Polymers for Immunofluorescence and In Vivo Imaging. *Bioconjugate Chem.* **2020**, *31*, 1497-1509.
52. Wang, W.; Ji, X.; Bin Na, H.; Safi, M.; Smith, A.; Palui, G.; Perez, J. M.; Mattoussi, H., Design of a Multi-Dopamine-Modified Polymer Ligand Optimally Suited for Interfacing Magnetic Nanoparticles with Biological Systems. *Langmuir* **2014**, *30*, 6197-6208.
53. De Roo, J.; Yazdani, N.; Drijvers, E.; Lauria, A.; Maes, J.; Owen, J. S.; Van Driessche, I.; Niederberger, M.; Wood, V.; Martins, J. C. et al., Probing Solvent-Ligand Interactions in Colloidal Nanocrystals by the NMR Line Broadening. *Chem. Mater.* **2018**, *30*, 5485-5492.
54. Anderson, N. C.; Hendricks, M. P.; Choi, J. J.; Owen, J. S., Ligand Exchange and the Stoichiometry of Metal Chalcogenide Nanocrystals: Spectroscopic Observation of Facile Metal-Carboxylate Displacement and Binding. *J. Am. Chem. Soc.* **2013**, *135*, 18536-18548.
55. Wang, W.; Ji, X.; Du, L.; Mattoussi, H., Enhanced Colloidal Stability of Various Gold Nanostructures Using a Multicoordinating Polymer Coating. *J. Phys. Chem. C* **2017**, *121*, 22901-22913.
56. Lakowicz, J. R., Principles of Fluorescence Spectroscopy. Third Edition ed.; Springer US: 2006.
57. Stoumpos, C. C.; Malliakas, C. D.; Peters, J. A.; Liu, Z.; Sebastian, M.; Im, J.; Chasapis, T. C.; Wibowo, A. C.; Chung, D. Y.; Freeman, A. J. et al., Crystal Growth of the Perovskite Semiconductor CsPbBr<sub>3</sub>: A New Material for High-Energy Radiation Detection. *Cryst. Growth Des* **2013**, *13*, 2722-2727.
58. Bertolotti, F.; Protesescu, L.; Kovalenko, M. V.; Yakunin, S.; Cervellino, A.; Billinge, S. J. L.; Terban, M. W.; Pedersen, J. S.; Masciocchi, N.; Guagliardi, A., Coherent Nanotwins and Dynamic Disorder in Cesium Lead Halide Perovskite Nanocrystals. *ACS Nano* **2017**, *11*, 3819-3831.

59. Cottingham, P.; Brutchey, R. L., On the crystal structure of colloiddally prepared CsPbBr<sub>3</sub> quantum dots. *Chem. Commun.* **2016**, *52*, 5246-5249.
60. Li, Z.-J.; Hofman, E.; Li, J.; Davis, A. H.; Tung, C.-H.; Wu, L.-Z.; Zheng, W., Photoelectrochemically Active and Environmentally Stable CsPbBr<sub>3</sub>/TiO<sub>2</sub> Core/Shell Nanocrystals. *Adv. Funct. Mater.* **2018**, *28*, 1704288.
61. Xia, Y.; Xia, X.; Peng, H.-C., Shape-Controlled Synthesis of Colloidal Metal Nanocrystals: Thermodynamic versus Kinetic Products. *J. Am. Chem. Soc.* **2015**, *137*, 7947-7966.
62. Zhong, Q.; Cao, M.; Xu, Y.; Li, P.; Zhang, Y.; Hu, H.; Yang, D.; Xu, Y.; Wang, L.; Li, Y. et al., L-Type Ligand-Assisted Acid-Free Synthesis of CsPbBr<sub>3</sub> Nanocrystals with Near-Unity Photoluminescence Quantum Yield and High Stability. *Nano Lett.* **2019**, *19*, 4151-4157.
63. Kirchnerová, J.; Cave, G. C. B., The solubility of water in low-dielectric solvents. *Can. J. Chem.* **1976**, *54*, 3909-3916.
64. Mai, B. T.; Barthel, M. J.; Lak, A.; Avellini, T.; Panaite, A. M.; Rodrigues, E. M.; Goldoni, L.; Pellegrino, T., Photo-induced copper mediated copolymerization of activated-ester methacrylate polymers and their use as reactive precursors to prepare multi-dentate ligands for the water transfer of inorganic nanoparticles. *Polym. Chem.* **2020**, *11*, 2969-2985.
65. Malhotra, K.; Fuku, R.; Chan, T. S.; Kraljevic, N.; Sedighi, A.; Piuono, P. A. E.; Krull, U. J., Bisphosphonate Polymeric Ligands on Inorganic Nanoparticles. *Chem. Mater.* **2020**, *32*, 4002-4012.
66. Giovanelli, E.; Muro, E.; Sitbon, G.; Hanafi, M.; Pons, T.; Dubertret, B.; Lequeux, N., Highly Enhanced Affinity of Multidentate versus Bidentate Zwitterionic Ligands for Long-Term Quantum Dot Bioimaging. *Langmuir* **2012**, *28*, 15177-15184.
67. Stelmakh, A.; Aebli, M.; Baumketner, A.; Kovalenko, M. V., On the Mechanism of Alkylammonium Ligands Binding to the Surface of CsPbBr<sub>3</sub> Nanocrystals. *Chem. Mater.* **2021**.
68. Kim, H.; Hight-Huf, N.; Kang, J.-H.; Bisnoff, P.; Sundararajan, S.; Thompson, T.; Barnes, M.; Hayward, R. C.; Emrick, T., Polymer Zwitterions for Stabilization of CsPbBr<sub>3</sub> Perovskite Nanoparticles and Nanocomposite Films. *Angew. Chem. Int. Ed.* **2020**, *59*, 10802-10806.
69. Cohen, T. A.; Huang, Y.; Bricker, N. A.; Juhl, C. S.; Milstein, T. J.; MacKenzie, J. D.; Luscombe, C. K.; Gamelin, D. R., Modular Zwitterion-Functionalized Poly(isopropyl methacrylate) Polymers for Hosting Luminescent Lead Halide Perovskite Nanocrystals. *Chem. Mater.* **2021**, *33*, 3779-3790.
70. Dey, A.; Ye, J.; De, A.; Debroye, E.; Ha, S. K.; Bladt, E.; Kshirsagar, A. S.; Wang, Z.; Yin, J.; Wang, Y. et al., State of the Art and Prospects for Halide Perovskite Nanocrystals. *ACS Nano* **2021**, *15*, 10775-10981.

**Table 1:** Summary of the various polysalt ligands synthesized and used for stabilizing the CsPbBr<sub>3</sub> PQDs. The relative molar fractions of the starting nucleophiles with respect to the PIMA monomers are compared side-by-side to the experimental values estimated from the <sup>1</sup>H NMR data.

Ligand	Molar ratio	Nominal number per chain <sup>a</sup>	Experimental number per chain from NMR <sup>b</sup>
<b>L1: AMB-PIMA-ODA<sup>c</sup></b>	x:y = 20:80	AMB: 8; ODA: 32	-
<b>L2: AMB-PIMA-OCA</b>	x:y = 20:80	AMB: 8; OCA: 32	AMB: ~8 OCA: ~ 31
<b>L3: AMB-PIMA-OCA</b>	x:y = 40:60	IMB: 16; OCA: 24	AMB: ~16 OCA: ~ 24
<b>L4: IMB-PIMA-ODA<sup>c</sup></b>	x:y = 20:80	IMB: 8; ODA: 32	- IMB:ODA ~ 1:4
<b>L5: IMB-PIMA-OCA</b>	x:y = 20:80	IMB: 8; OCA: 32	IMB: ~9 OCA: ~ 31
<b>L6: IAB-PIMA-OCA</b>	x:y = 40:60	IMB: 16; OCA: 24	IMB: ~14 OCA: ~26

<sup>a</sup> The reported values were obtained from the molar concentration of the amine-modified precursors, compared to that of the monomers in PIMA.

<sup>b</sup> The values were obtained by comparing the <sup>1</sup>H NMR peak integration of ammonium dimethyl ( $\delta \sim 3$  ppm), imidazolium ( $\delta \sim 9.2$  ppm) and OCA ( $\delta \sim 0.85$  ppm) to the two methyl groups in the polymer backbone ( $\sim 234$  H,  $\delta \sim 0.97$  ppm). Spectral deconvolution was applied to resolve the overlapping peaks in the range of 0.8-1 ppm and extract the integration values.

<sup>c</sup> Note that we have not attempted to extract accurate stoichiometry data for **L1: AMB-PIMA-ODA** and **L4: IMB-PIMA-ODA**, due to the strong overlap between the signatures of the alkyl chains and the dimethyl groups in PIMA.

**Table 2.** PL lifetime and PLQY acquired from dispersions of PQDs with different coatings. The lifetime values are reported together with the lifetime ratios measured for the polysalt- and OLA/OA-PQDs.

PQDs	Lifetime, $\tau$	Lifetime ratio	PLQY	PL <sub>normalized</sub>
OLA/OA-PQDs	7.9 ns	1	~65%	1
<b>L1-PQDs</b>	8.8 ns	1.11	~90%	1.55
<b>L4-PQDs</b>	10.0 ns	1.27	~95%	1.62
<b>L2-PQDs</b>	10.4 ns	1.32	~94%	1.51
<b>L5-PQDs</b>	10.6 ns	1.34	~98%	1.55